Pis'ma v ZhETF, vol. 82, iss. 11, pp. 791 – 796

X-ray detected magnetic resonance at the Fe K-edge in YIG: forced precession of magnetically polarized orbital components

J. Goulon, A. Rogalev[1)], *F. Wilhelm, N. Jaouen, C. Goulon-Ginet, G. Goujon, J. Ben Youssef*[+], *M. V. Indenbom*[+]

European Synchrotron Radiation Facility (ESRF), B.P.220, 38043 Grenoble Cedex, France

[+]*Laboratoire de Magnétisme de Bretagne, CNRS FRE 2697, UFR Sciences et Techniques, 29328 Brest Cedex 03, France*

Submitted 20 October 2005

X-ray Detected Magnetic Resonance (XDMR) has been measured for the first time on exciting the Fe K-edge in a high quality Yttrium Iron Garnet film epitaxially grown on a Gadolinium Callium Garnet substrate. This challenging experiment required resonant pumping of Yttrium Iron Garnet at high microwave power, *i.e.* in the *foldover* regime. X-ray Magnetic Circular Dichroism (XMCD) was used to probe the change in the longitudinal component of the magnetization M_Z induced by the precession of magnetic moments located at the iron sites. Since XMCD at the Fe K-edge refers mostly to the equilibrium contribution of magnetically polarized $4p$ orbital components, XDMR at the Fe K-edge should reflect the precessional dynamics of the latter orbital moments. From the measured precession angle, we show that there is no dynamical quenching of the polarized orbital components at the iron sites in Yttrium Iron Garnet.

PACS: 75.25.+z, 76.50.+g, 78.20.Ls, 78.47.+p

X-ray Magnetic Circular Dichroism (XMCD) [1, 2] has become a well established tool to study orbital magnetism in thin films and metallic multilayers. The element/edge selectivity of XMCD proved itself to be very helpful to study induced magnetism [3] whereas sum-rules at spin-orbit split edges made it possible to resolve the contributions of spin and orbital moments [4 – 6]. We show below that XMCD can also be used to probe the resonant precession of the magnetization caused by a strong microwave *pump* signal. X-ray Detected Magnetic Resonance (XDMR) is then a peculiar transposition into the X-ray regime of Optically Detected Magnetic Resonance (ODMR) [7 – 9].

Very recently, precessional motions of elemental spin moments were measured by Bailey et al.[10] who recorded time-resolved X-ray differential circular reflectivity spectra at the L-edges of Fe and Ni in Permalloy. This could be an alternative approach to the same physics even though time-domain measurements are still restricted to low frequency resonances. At the ESRF [11], efforts were focused on detecting XDMR in the *frequency* domain: beamline ID12, which is equipped with helical undulators producing intense beams of circularly polarized X-rays, has now the capability to record XDMR spectra under high microwave pumping power at frequencies ranging from 1 to 18 GHz. The XDMR experiment reported below was performed in the microwave X-Band, slightly below 10 GHz. The energy range (1.8–18 keV) covered by beamline ID12 allows the ESRF users to access to the X-ray absorption K-edges of all $3d$ transition metals, the L-edges of all rare-earths as well as all $4d$ and $5d$ transition elements.

Whereas the Landau-Lifschitz-Gilbert (LLG) equation is classically used to describe the precession of the *effective* magnetization in conventional Ferro-Magnetic Resonance (FMR) [12], we proposed elsewhere[13] to use it to describe the precession of *local* magnetic moments. A distinction was made between two configurations: in the *longitudinal* geometry illustrated with Fig.1, the wavevector $\mathbf{k}_X(\|)$ of the incident, circularly

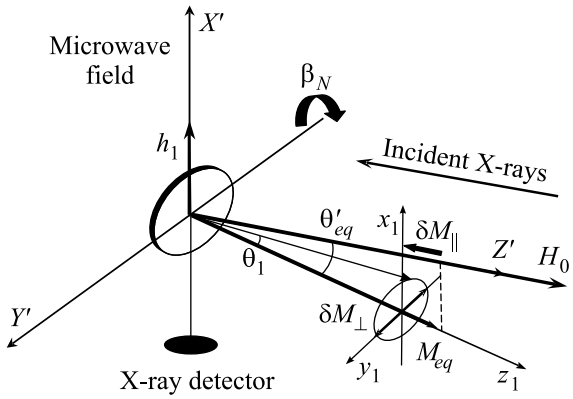

Fig.1. XDMR in longitudinal geometry; see text for notations

polarized X-rays is parallel to the static bias field $\mathbf{H_0}$, whereas in a *transverse* geometry, the wavevector $\mathbf{k}_X(\perp)$ would be perpendicular to $\mathbf{H_0}$. It was recognized first

[1)] e-mail: rogalev@esrf.fr

by Bloembergen and Damon [14] that the longitudinal geometry was much less sensitive to magnon-magnon scattering processes and provided a higher saturation limit with respect to the incident microwave power. Experimentally, the longitudinal geometry benefits of the major simplification that there is no need for fast X-ray detectors because the XDMR signal is expected to be proportional to the microwave power that can be conveniently amplitude modulated at low frequency. In a transverse geometry, the precession of the magnetic moments induces a XMCD signal oscillating at the microwave resonance frequency and the detection of such a fast modulation of the X-ray absorption cross-section requires a more sophisticated electronics still under test. In both configurations, the XMCD/XDMR signals are systematically recorded in the X-ray fluorescence excitation mode.

The key information which we want to extract from a XDMR experiment is the precession angle of the local magnetic moments in the *uniform* mode regime. This led us to solve the polar LLG equations of motion in the true precession frame in which $\mathbf{M}(\theta_1, \phi_1)$ deviates from its equilibrium position $\theta_1 = 0$ when a microwave field $\mathbf{h_1}$ perpendicular to $\mathbf{H_0}$ is switched on. As illustrated with Fig.1, the sample, i.e. a Yttrium Iron Garnet (YIG) film, was slightly tilted with the consequence that the direction of the equilibrium magnetization $\mathbf{M}_{eq}(\theta'_{eq}, \phi'_{eq})$ did not coincide with the direction of $\mathbf{H_0}$: Euler angles ($\alpha_0 = \phi'_{eq}$, $\beta_0 = \theta'_{eq}$, $\gamma_0 = 0$) describe the rotation transforming the laboratory frame into the precession frame of Fig.1. Let us restrict our analysis to *steady state* solutions of the LLG equations satisfying the conditions: $d\theta_1/dt = 0$ and $\phi_1 = \omega t + \phi_{1_0}$. Therefore, the precession angle θ_{1_0} should not depend on the azimuthal angle ϕ_1 which is time-dependent. For a microwave field h_{1cp} circularly polarized in the (X', Y') plane, one obtains [13]:

$$\tan^2\theta_{1_0} = \frac{1}{4}[1+\cos\beta_0]^2 \frac{(\gamma\mu_0 h_{1cp})^2}{(P_{1_0})^2 + (Q_{1_0}\cos\theta_{1_0})^2} \quad (1)$$

in which γ denotes the gyromagnetic ratio. We also introduced the simplifying notations:

$$P_{1_0} = \gamma\mu_0 H_0 \cos\beta_0 - \mu_0\omega + \frac{\gamma}{M_s \sin\theta_{1_0}} \frac{\partial F_{AD_{\ell,m=0}}}{\partial\theta_1}, \quad (2)$$

$$Q_{1_0} = -\mu_0\alpha\omega - \frac{\gamma}{M_s \sin^2\theta_{1_0}} \frac{\partial F_{AD_{\ell,m=0}}}{\partial\phi_1} \equiv -\mu_0\alpha\omega, \quad (3)$$

in which $F_{AD_{\ell,m}}$ is the sum over all relevant terms of the spherical harmonics expansion of $F_{AD}(\theta_1, \phi_1)$ which regroups the magnetic anisotropy free energy (F_A) plus the demagnetizing free energy (F_D). Small harmonic distortions of the precession trajectories should be expected due to the neglected terms $\Delta F_{AD_{\ell,m\neq 0}}$. Such distortions are a source for *inhomogeneous* FMR line broadening and justify the addition of a frequency independent damping term to Q_{1_0} that should increase with the tilt angle (β_N). It should remain negligible whenever $\theta'_{eq} = 0$ and $\theta_{1_0} \equiv \theta'_0$. Using standard notations for a uniaxial film:

$$P_{1_0} \to P'_0 = -\mu_0\omega + \gamma\mu_0 H_0 + \gamma[2K_u/M_s - \mu_0 M_s]\cos\theta'_0$$

whereas $Q_{1_0} \to Q'_0 = -\mu_0\alpha\omega$. Under such conditions, equation (1) becomes:

$$\tan^2\theta'_0 = \frac{(\gamma\mu_0 h_{1cp})^2}{P'^2_0 + (Q'_0\cos\theta'_0)^2}, \quad (4)$$

This is precisely the result derived by Gnatzig et al. for ODMR [9]. In practice, $\cos\theta_{1_0}$ or $\cos\theta'_0$ can be extracted numerically either from (1) or (4): the spectral dependence of the precession angles is thus characterized by non-Lorentzian *foldover* lineshapes [9], as predicted by Weiss [15] in cases of large shape or crystalline magnetic anisotropies.

In the XDMR experiment described below, XMCD is used to probe the small changes in the magnetization caused by the precession of local magnetic moments around the *effective* field:

$$\delta M_{\|}^{(0)} = M_s[\cos\theta_{1_0} - 1] \simeq -\frac{1}{2}\tan^2\theta_{1_0} M_s. \quad (5)$$

In the longitudinal geometry of Fig.1, the differential X-ray absorption cross section $\Delta\sigma$ should exhibit a non-oscillating component given by:

$$\Delta\sigma^{(0)}_{XDMR}(k_{\|}) = [\Delta\sigma_{XMCD}(k_{\|})]_{eq}(\cos\theta'_0 - 1) \simeq$$
$$\simeq -\frac{1}{2}\tan^2\theta_{1_0}[\Delta\sigma_{XMCD}(k_{\|})]_{eq}. \quad (6)$$

Combined measurements of XDMR and XMCD cross sections in the same geometry should thus allow us to determine the precession angle θ_{1_0} of the magnetic moments at the specific site of the X-ray absorbing element.

Our sample was a thin film of YIG (8.9 μm thick) grown by liquid phase epitaxy along the (111) direction of the Gadolinium Gallium Garnet substrate (film $N°520$). As a preamble to any XDMR experiment, conventional (transverse) FMR spectra had to be recorded. The ESRF microwave bridge is equipped with a wide-band, low-noise generator (*Anritsu* MG-3692) and its master piece is a fully integrated phase discriminator

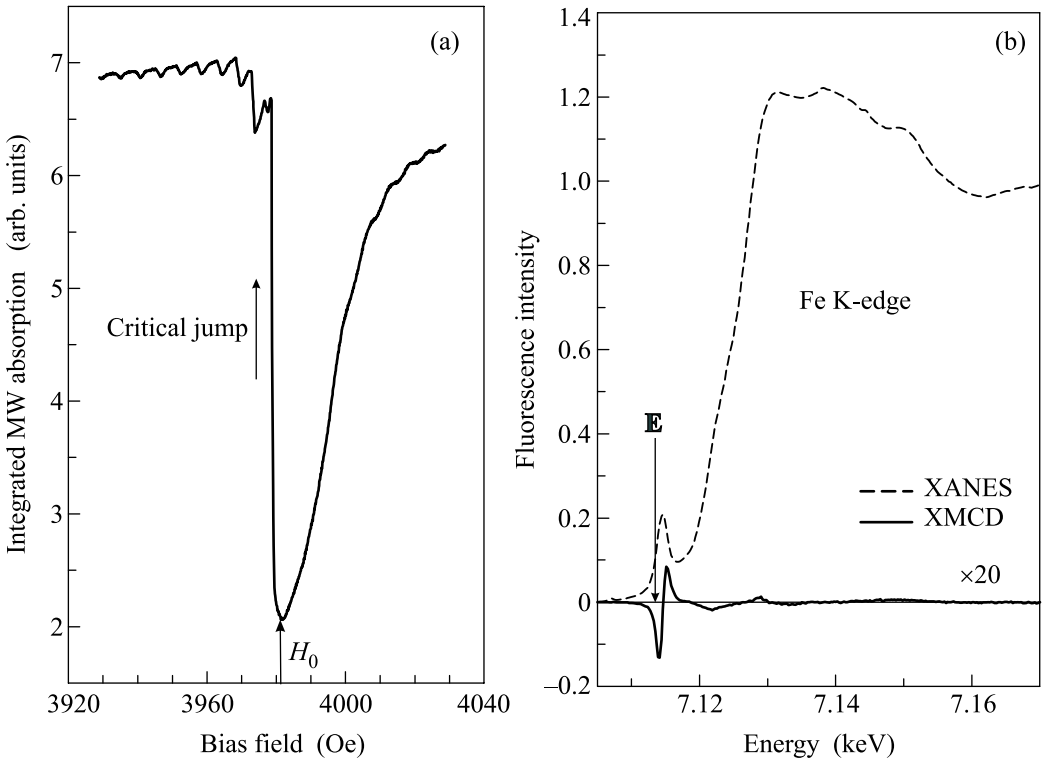

Fig.2. XDMR settings: (a) resonant pumping near the critical foldover jump; (b) XMCD probe

(*Anaren* 20758). The microwave power (≤ 32 dBm) delivered by a solid-state low noise amplifier (*Miteq* AMF-4B) was high enough to pump efficiently our high quality YIG film. For XDMR, the microwave power was square modulated using a fast switch (SPST: *Miteq* 124796: 80 dB isolation; rise/decay times ≤ 2 ns). The sample ($2 \times 2\,\mathrm{mm}^2$) was glued on a low-loss sapphire rod (Ø4 mm) terminated by a flat surface slightly tilted from the rod axis. This sample holder was inserted in a rectangular TE_{102} X-band cavity ($F_{\mathrm{cav}} \approx 9450$ MHz; $Q_L \leq 4300$) which was itself located in a high-vacuum, amagnetic stainless steel chamber connected to the beamline. What makes this cavity non-standard with respect to commercial electron paramagnetic resonance cavities is: (i) the need to drill a hole (Ø3 mm) to let the X-ray beam propagate inside the cavity along the axis of the external modulation coils; (ii) the presence at the bottom of the cavity of an X-ray detector collecting the X-ray fluorescence photons in as large a solid angle as possible. This detector is a PNN^+ Si photodiode optimized by *Canberra-Eurisys* to keep a low capacitance (≤ 11 pF) while offering a large active area. It had to be carefully shielded and protected by an ultra-thin Be window in order to prevent any direct detection of microwaves. Much attention was also paid to avoid leaks of radiated microwaves outside the cavity: this led us to add another thin Be window to mask the coupling hole of the incoming X-rays. The detector readout electronics combined a home-made, magnetically shielded, ultra-low noise preamplifier with a multichannel Vector Spectrum Analyzer (*Agilent* VSA 89600-S) exploiting 23-bits digitizers. The dynamic range of our detector was checked to exceed 126 dBc.

All FMR spectra recorded with the magnetic field $\mathbf{H_0}$ perpendicular to the film plane exhibited a rich pattern of narrow lines ($\Delta H_{pp} \leq 0.5$ Oe) due to magnetostatic modes. However, even at very low incident microwave power, the resonance of the uniform mode vanished due to a very high *radiation damping* effect. To recover a strong signal, we used two tricks: (i) the cavity was overcoupled ($Q_L \approx 800$); (ii) the microwave frequency was offset by up to 50 MHz with respect to the cavity resonance frequency. As expected, the linewidth of the uniform mode was found to increase quite significantly as a function of the tilt angle β_N between the normal of the sample and the direction of $\mathbf{H_0}$. For a sample normally magnetized, the linewidth $\Delta H_{fwhm}(\beta_N = 0^\circ) = \sqrt{3}\Delta H_{pp}$ was only 1.13 Oe. ΔH increased to 1.21 Oe for $\beta_N = 6^\circ$; 2.16 Oe for $\beta_N = 16^\circ$ and finally 3.64 Oe for $\beta_N = 30^\circ$. Even though other extrinsic contributions cannot be excluded, much of this inhomogeneous broadening may be due to highly distorted precession

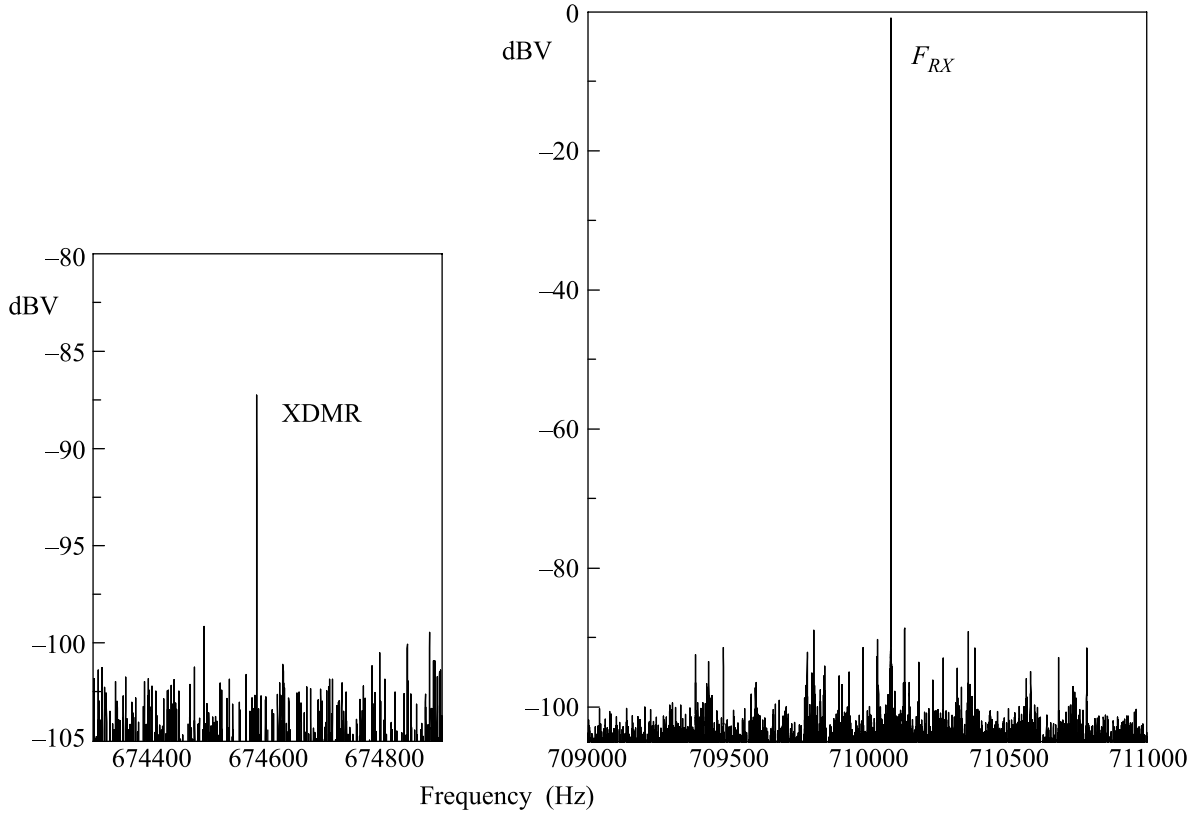

Fig.3. XDMR signal as low-frequency side-band of F_{RX}

trajectories. We also measured carefully the linear dependence of the linewidth as a function of the microwave frequency over the restricted range (8.2–10.5 GHz) in order to determine the *intrinsic* linewidth from the slope: 0.04 Oe/GHz. This figure is nearly identical to the value derived by Charbois [16] for another YIG film prepared under fairly similar conditions. It may be converted into a Gilbert damping factor of ca. $6.0\,10^{-5}$ which confirms the high quality of the YIG film prepared in Brest.

The XDMR experiment was carried out with a film inclined at $\beta_N = 30°$ in order to prevent the X-ray fluorescence to be re-absorbed. The microwave frequency (9445.0 MHz) was offset by only 5 MHz with respect to the resonance of the overcoupled cavity. The incident microwave power was increased up to 30 dBm and was large enough to saturate the *transverse* FMR spectrum but not the ΔM_Z spectrum [16]: the angular foldover regime was unambiguously reached. Nevertheless, Gnatzig et al. [9] and others [16] emphasized that the maximum precession angle $\theta_{\max}$ is *never* reached with amplitude modulated microwaves: what is detected experimentally is at best a foldover critical jump which occurs at $\theta_{\text{critical}} < \theta_{\max}$. As illustrated with Fig.2a, the resonance field was scanned down to the onset of the critical foldover jump observed at $\mathbf{H_0} = 3980.6$ Oe. As explained by Fig.2b, the energy of the incident X-rays was tuned to 7113.74 eV which corresponds to the maximum of the XMCD signal in the pre-peak of the X-ray Absorption Near Edge (XANES) spectrum. Since the ESRF storage ring was run in the $2 \cdot 1/3$ filling mode, the incident X-rays were modulated at the macrobunch repetition frequency ($F_{RX} = 710.084$ kHz) and the microwave modulation at $F_m = 35.5042$ kHz was triggered using the radiofequency master clock. Spectra collection was performed in a synchronous *time-average mode* of the VSA using a triggering signal at F_m.

The XDMR signal reproduced in Fig.3 is one of the modulation side-bands expected at $710.084 \pm$ $\pm$ 35.5042 kHz. The signal at F_{RX} was used only for monitoring the X-ray fluorescence intensity and data renormalization. Let us stress that the noise floor in Fig.3 is well above the intrinsic detector noise: it reflects mostly the statistical (white) noise of the X-ray source. The *magnitude* of the XDMR signal is peaking *ca.* 20 dBV above the noise floor. Fig.4 displays the real and imaginary parts of the spectrum: the XDMR signal, just like XMCD, gets nicely inverted when the undulator phase is inverted, *i.e.* when the helicity of the

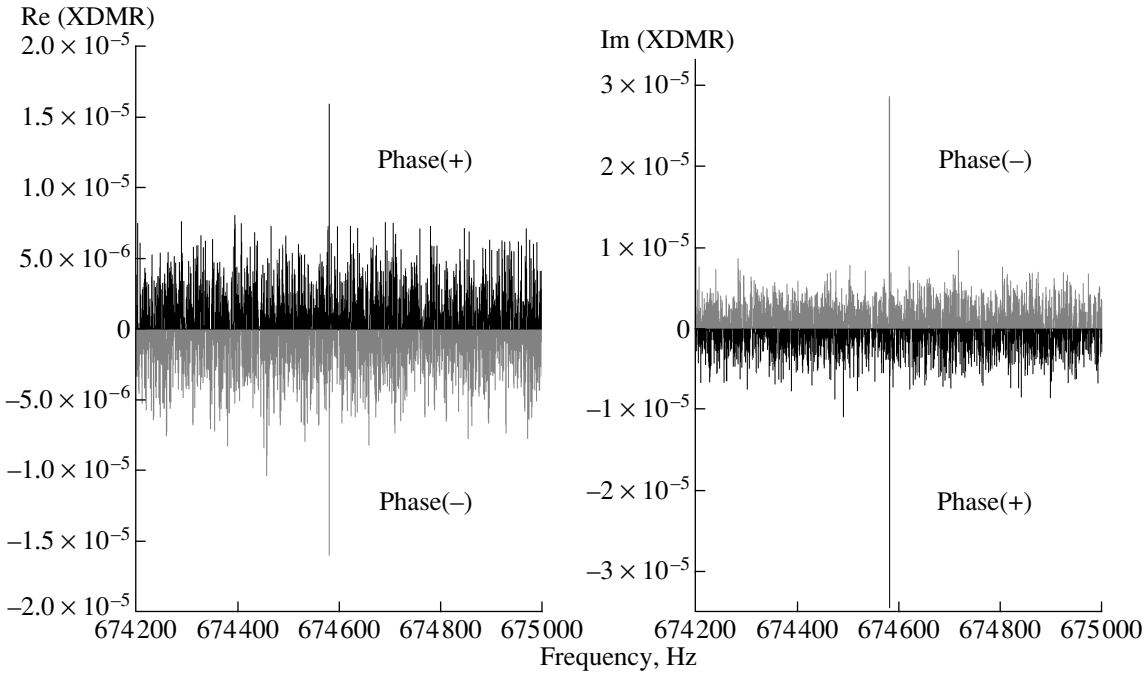

Fig.4. Inverted XDMR on switching the X-ray helicity from left (phase (+)) to right (phase (−))

incident X-ray beam is changed from left to right. There is a minor change in intensity which strictly reproduces the change in the fluorescence intensity monitored by the peak at F_{RX}. After proper renormalization with respect to the edge-jump, we obtained a small differential cross-section: $\Delta\sigma_{XDMR} \approx 1.34 \cdot 10^{-5}$ which, according to (6), would yield a critical angle of $\theta_{1_0} \approx 3.5^\circ$ for the precessing moments at the Fe sites.

The differential form of the XMCD sum rules derived by Ebert et al. [6] for electric dipole $1s \rightarrow 4p$ ($E1$) transitions shows that the effective operators describing XMCD at a K-edge is purely of orbital nature. According to Carra et al.[17], this should still hold true for the weak contribution of electric quadrupole $1s \rightarrow 3d$ ($E2$) transitions in the pre-edge. The effective operator accounting for XMCD at the Fe K-edge could then be written: $\frac{d}{dE}[\langle L_z\rangle_{4p} + \epsilon\langle L_z\rangle_{3d}]$, the two terms reflecting the respective contributions of $E1$ and $E2$ transitions. Fe K-edge XDMR thus produces clear evidence of the forced precession of *orbital* polarization components.

It was desirable to determine as well the precession angle of the *effective* moments responsible for FMR: in YIG, those are essentially the spin moments of the ferrimagnetically coupled iron sublattices with $g_{\text{eff}} = 1.997$. The main difficulty in expoiting (1) or (4) is to determine h_{1cp}. Following standard textbooks, e.g. [18], h_{1cp} in a TE_{102} cavity should be given by:

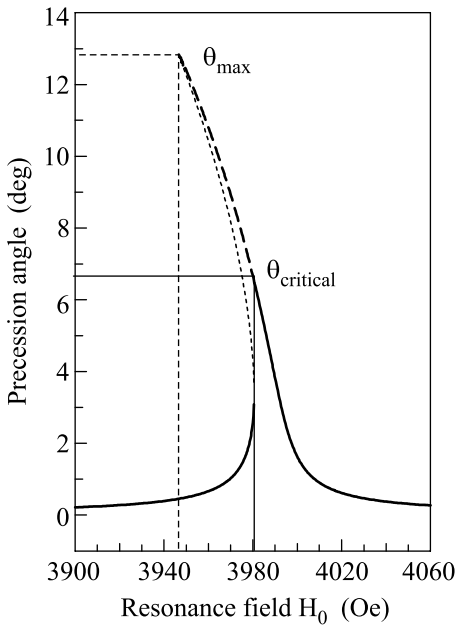

Fig.5. Simulated angular foldover for the precession of the effective spins in YIG

$$[h_{1cp}]^2 = \frac{10Q_L}{F_{MW}(GHz)V_{\text{cav}}(mm^3)}\frac{8(1-|\Gamma|^2)}{1+(L/2a)^2}P_{\text{inc}}(W),$$

where L is the cavity length, $2a$ the cutoff wavelength and $|\Gamma|^2$ the magnitude of the reflection coefficient measured with a vector network analyser. In order to account for the frequency offset, we used an effective Q_L

yielding $h_{1cp} \approx 371\,\mathrm{mOe}$ for $P_{\mathrm{inc}} = 1$ W. This result had to be corrected for the strong radiation damping effect in YIG. From an independent determination of the line broadening ($\Delta H_{RD} = 0.68\,\mathrm{Oe}$), and following the same correction procedure as discussed by Charbois [16], we finally obtained $h_{1cp} \approx 335\,\mathrm{mOe}$. Fig.5 reproduces the angular foldover lineshape simulated according to (1) if one adds to the Gilbert damping term another term accounting for the inhomogeneous linewidth ($\Delta H_{\mathrm{inh}} = 2.6\,\mathrm{Oe}$). Note that the critical precession angle $\theta_{\mathrm{crit}} = 6.8^\circ$ is *ca.* one half of θ_{max}. Let us emphasize that the precession angle θ_{1_0} deduced from XDMR for the orbital polarization components is only one half of the critical precession angle θ_{crit} of the effective spin moment. Since the electron gyromagnetic ratios for orbital and spin moments are precisely in a 1:2 ratio, our XDMR result proves that, in YIG, there is *no* dynamical quenching of the magnetic orbital polarization components: spin-orbit coupling dominates orbit-lattice interactions in Kittel's picture of FMR.

The authors greatly appreciated the support of Y. Petroff (ESRF) and M. P. Klein (LBL , CA.) in the early stage of the project. Technical assistance by S. Feite and P. Voisin is also warmly acknowledged.

1. G. Schütz et al., Phys. Rev. Lett. **58**, 737 (1987).
2. C. T. Chen et al., Phys. Rev. B **42**, 7262 (1990).
3. F. Wilhelm et al., Phys. Rev. Lett. **87**, 207202 (2001).
4. B. T. Thole et al., Phys. Rev. Lett. **68**, 1943 (1992).
5. P. Carra et al., Phys. Rev. Lett. **70**, 694 (1993).
6. H. Ebert, V. Popescu, and D. Ahlers, Phys. Rev. B **60**, 7156 (1999).
7. J. T. Hanlon and J. F. Dillon, J. Appl. Phys. **36**, 1269 (1965).
8. A. S. Borovik-Romanov et al., J. Phys. C: Solid St. Phys. **13**, 875 (1980).
9. K. Gnatzig et al., J. Appl. Phys. **62**, 4839 (1987).
10. W. E. Bayley et al., *Phys. Rev. B* **70**, 172403 (2004).
11. J. Goulon, F. Sette, W. G. Stirling in: *Emerging scientific opportunities at the ESRF*, Medium-Term Scientific Programme for the period 2003-2007, 2002.
12. A. G. Gurevich and G. A. Melkov, *Magnetization Oscillations and Waves*, CRC Press Boca Raton, Inc., 1996.
13. J. Goulon et al., *XDMR in thin films: 1. Uniform mode regime*, to be submitted.
14. N. Bloembergen and R. W. Damon, Phys. Rev. **85**, 699 (1952).
15. M. T. Weiss, Phys. Rev. Lett. **1**, 239 (1958).
16. V. Charbois, *Ph.D. Thesis*, Université Paris VII, 2003.
17. P. Carra et al., Physica B **192**, 182 (1993).
18. C. P. Poole, *Electron Spin Resonance*, Wiley – Interscience, New-York, 1967.